Available online at www.sciencedirect.com
SCIENCE DIRECT
International Journal of Heat and Mass Transfer 49 (2006) 951–961
International Journal of HEAT and MASS TRANSFER
www.elsevier.com/locate/ijhmt

MRI investigation of the evaporation of embedded liquid droplets from porous surfaces under different drying regimes

N.C. Reis Jr. [a,*], R.F. Griffiths [b], M.D. Mantle [c], L.F. Gladden [c], J.M. Santos [a]

[a] Departamento de Engenharia Ambiental, CT-UFES, Av. Fernando Ferrari, S/N, CEP 29060-970, Vitória-ES, Brazil
[b] Environmental Technology Centre, Department of Chemical Engineering, UMIST, P.O. Box 88, M60 1QD, UK
[c] Department of Chemical Engineering, University of Cambridge, Pembroke Street, Cambridge, CB2 3RA, UK

Received 21 September 2004; received in revised form 20 August 2005
Available online 22 November 2005

Abstract

A combination of in situ one-dimensional ^{1}H magnetic resonance profiling and two-dimensional imaging has been applied to study the shape and subsequent dynamic evaporation behaviour of a single liquid droplet after impact onto a porous surface. Diethyl-malonate (DEM) droplets are initially embedded in the porous substrate by impingement, and are then evaporated over a period of several hours; the surface of the substrate being ventilated by a controlled airflow. The configuration is intended to mimic the behaviour of droplets evaporating into atmospheric flows. In order to evaluate the influence of the airflow at the surface of the porous medium, different experimental configurations were tested by varying the speed of the airflow stream above the porous surface. The method produces several types of data, including images of impinged droplets inside the porous substrate and their development with time during the evaporation episode, one-dimensional concentration profiles through the substrates, and corresponding estimates of the mass fraction of liquid remaining, evaporation rate and mass flux per unit area. The results obtained show that although liquid droplets tend to evaporate faster and present larger evaporation rates when exposed to a more efficient removal of vapour from the surface, the limiting effects of the porous medium are even more evident.

1. Introduction

The study of the impact and evaporation of liquid droplets on porous surfaces is important for a wide range of situations, varying from environmental applications to inkjet printing technology. When a liquid droplet collides with a permeable surface it resides in the porous medium in a shape similar to a half-spheroid, whose aspect ratio will depend on the porous medium and liquid droplet characteristics [1]. Once the droplet is embedded in the porous substrate, its evaporation is dependent not only on the thermodynamic parameters affecting the rate of conversion from one phase to another, but also on the parameters affecting the mass transport mechanisms (of liquid and vapour) inside the porous substrate and the removal of vapour from the contaminated surface in the atmosphere/porous medium interface.

One of the first reported attempts to investigate droplet impact and evaporation on permeable surfaces was performed by Wallace and Yoshida [2], and was motivated by the analysis of the efficacy of pesticide spray. Subsequently, a series of studies on the subject were reported, motivated by inkjet printing technology [3,4] and hazard assessment purposes of liquid releases in the atmosphere [5–8]. These studies have reported laboratory, wind tunnel and field experiments investigating the governing parameters of the problem, such as porous medium properties (porosity and particle size), liquid properties, and the efficiency of the removal of vapours from the porous/atmosphere interface (wind speed and turbulence).

Although these studies presented detailed experimental investigations of the phenomenon, there was very little

* Corresponding author.
E-mail address: neyval@inf.ufes.br (N.C. Reis Jr.).

0017-9310/$ - see front matter © 2005 Elsevier Ltd. All rights reserved.
doi:10.1016/j.ijheatmasstransfer.2005.09.014

Nomenclature

A	area (m^2)
c	integrated concentration along the horizontal plane (kg/m)
c_s	vapour concentration at the surface of the porous medium (kg/m^3)
c_r	vapour concentration in the air stream (kg/m^3)
c_{sat}	value of the saturated vapour concentration in air (kg/m^3)
$c_{sat-liq}$	value of the saturated liquid concentration for the porous medium (kg/m^3)
dM/dT	evaporation rate (kg/s)
F	mass flux to the air stream ($kg/s\,m^2$)
M	mass of the liquid (kg)
r	droplet radius (m)
T	time (s)
u_*	friction velocity of the air stream (m/s)
v_r	vapour transfer velocity to the air stream (m/s)
x	coordinate along the axis of the test tube, i.e. depth of the porous substrate (m)
y	coordinate along the radius of the test tube (m)

Subscript

0	reference value

Superscript

*	non-dimensional value

information about the shape of the liquid droplet and the behaviour of the liquid inside the porous medium. Reis et al. [9] carried out the first studies using magnetic resonance imaging (MRI) techniques to follow the behaviour of single water droplets evaporating from porous surfaces. The experimental configuration was intended to mimic the behaviour of droplets evaporating into atmospheric flows from various porous surfaces. The results indicated that the transport of liquid by capillary diffusion has a very strong influence upon the evaporation process, providing a challenge to the simple receding evaporation-front assumption that is utilised in many modelling procedures [1,7].

Although the paper by Reis et al. presents a considerable amount of information, it does not investigate the influence of the airflow over the interface atmosphere/porous medium, which is one of the main factors governing the phenomenon and can considerably alter the drying regime [7]. Further information is necessary to evaluate the importance of liquid transport under different drying regimes to substantiate and validate model development. Accordingly, the aim of this work is to study the influence of the airflow over the surface of the porous medium, and to provide information about the behaviour inside the porous medium.

In order to achieve this objective, a magnetic resonance imaging study was carried out to provide images of the shape of droplets inside the porous medium after the impact and throughout the evaporation episode. A carefully adjusted airflow is established over the porous surface, in order to ventilate the surface and produce a mass flux similar to that in the atmosphere. The results indicate distinct differences in the drying regimes as the airflow rate and the liquid properties are changed.

Accordingly, the results presented in this paper are divided into three main sections: (i) an analysis of the accuracy of the simulation of the atmospheric conditions provided by the controlled airflow during the evaporation episode by comparing the results obtained with field observations [10], (ii) comparison of the drying regimes obtained for water droplets [9] and DEM droplets under similar evaporation conditions and (iii) analysis of the influence of the removal of vapour from the atmosphere/porous medium interface.

2. Experimental set-up and procedure

As discussed in the previous section, the experimental procedure described here tries to mimic atmospheric conditions inside the MRI magnet, where the evaporation process can be monitored and imaged. The droplets were initially embedded in the porous substrate by impingement, and then evaporated over a period of several hours, the surface of the substrate being ventilated by a controlled airflow. In order to investigate influence of the airflow over the surface of the porous medium, and to provide information about the behaviour inside the porous medium, the flow rate of the airflow was varied.

The following sections contain a description of the experimental set-up and experimental procedure used in this study, as well as a brief discussion of the procedures used to approximately simulate atmospheric conditions.

2.1. Experimental set-up

All MRI acquisitions were performed using a Bruker DMX-300 spectrometer operating at a ^1H (proton) frequency of 300.13 MHz corresponding to a static magnetic field strength of 7.07 T. One-dimensional profiles and two-dimensional images were acquired using a 15 mm diameter birdcage radiofrequency resonator. These dimensions restrict the maximum sample holder/set-up diameter to 14 mm. Spatial resolution was achieved using 3-orthogonal axis (x, y and z) actively shielded gradient system capable of producing a maximum gradient strength of $1\ T\ m^{-1}$ in all three cartesian directions. An experimental

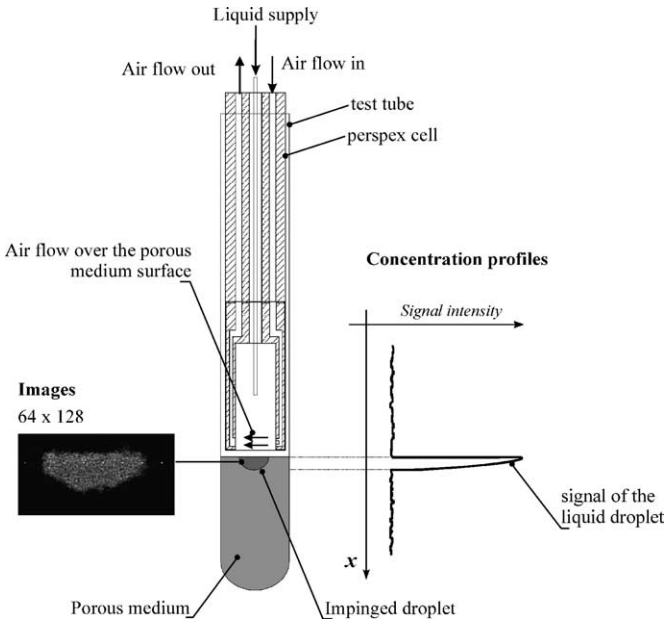

Fig. 1. Detailed view of a longitudinal section of the cell placed inside the test tube containing the porous substrate, with a schematic representation of a lateral (zx-slice) two-dimensional image of the liquid droplet just after impingement and a corresponding liquid concentration profile.

cell was built to provide the required ventilation airflow within this limited space. The ventilation cell consists of a Perspex tube and a flange, containing three internal orifices: one to supply the inlet airflow, another to allow the outlet airflow and a third used to place a capillary tube close to the porous surface and deliver the droplet (Fig. 1).

The experimental procedure involves partially filling a test tube with a porous material (e.g. sand or glass beads), in order to obtain a well-defined porous layer (Fig. 1). The ventilation cell is then carefully lowered down the bore of the magnet so that it is just in contact with the surface of the porous substrate. A capillary tube was used to deliver a liquid droplet of diethylmalonate (Sigma Aldrich, UK) to the porous substrate. After the droplet had been delivered to the substrate an airflow was maintained via the inlet and outlet orifices, creating an airflow parallel to the porous surface. The sample and air flow were maintained at a temperature of 297.5 ± 0.5 K during the evaporation episode.

2.1.1. Determination the flow rate of the air supply

In the initial stages of the droplet evaporation, all the pores in the surface of the wetted spot are saturated and the flux to atmosphere is totally controlled by the transport phenomena in the atmosphere/porous medium interface. As the evaporation proceeds and the pores on the surface of the substrate start to dry out, the process becomes more and more dependent on the transport inside the porous medium. Therefore, in order to simulate evaporation under atmospheric conditions, the air supply must be carefully controlled. However, it is not possible to simulate the turbulence levels and the pattern of the air flow in the atmosphere inside such a small apparatus. Nevertheless, the fluid flow does not need to be exactly the same as in the atmosphere, since the crucial factor is the magnitude of the mass flux through the surface of the porous medium. If the flow velocity inside the cell is carefully adjusted, it is possible to approximately match the mass flux expected under given atmospheric conditions and the mass flux obtained in the cell. If this matching is achieved, the phenomena displayed within the porous medium in the NMR experiment should be representative of those occurring in a field situation.

The mass flux to the air stream is usually parameterised as [1]:

$$F = v_r(c_s - c_r) \tag{1}$$

where F denotes the mass flux to the air stream (kg/m^2 s), v_r is the vapour transport velocity (m/s), c_s is the vapour concentration at the surface (kg/m^3) and c_r is the vapour concentration (kg/m^3) in the air stream. The value of c_r is usually taken to be equal to zero, as the background concentration is often neglected [7,13]. The value of v_r is mainly dependent on the characteristics of the airflow (especially the friction velocity).

In the initial stages of the evaporation process, all the pores in the surface are full of liquid, and the vapour concentration in the surface is equal to the saturated vapour concentration in the air. As the evaporation proceeds and the pores on the surface of the substrate start to dry out, the value of c_s starts to be reduced and becomes dependent on the transport inside the porous medium.

By using this parameterisation, the mass flux to the air stream can be treated as a convective transport of vapour, with characteristic velocity v_r determined by the transport mechanisms through the air stream/porous surface interface. According to Roberts and Griffiths [7], the value of v_r for the atmosphere is mainly dependent on the friction velocity (u_*) of the approaching flow. For droplets evaporating exposed to atmospheric flows, the value of v_r ranges from 0.02 to 0.15 m/s, depending on the wind velocity and turbulence conditions (these values are based on expressions presented in [7]).

The ventilation cell used in the experiments was built with the intent of providing an air stream parallel to the surface of the porous substrate. However, a completely parallel airflow is very difficult to obtain due to the limited dimensions inside the test tube and the complex geometry required to deliver the air supply. These limitations create great difficulties in describing the airflow and the mass flux over the porous surface inside the cell. In order to overcome these problems, and to estimate the mass flux inside the cell, a computational fluid dynamics (CFD) model is used. In order to determine the value of v_r inside the cell, and thereby to simulate evaporation of droplets exposed to the atmosphere, a computational fluid dynamics (CFD) model of the fluid flow inside the cell was developed (for a description of the CFD model the reader is referred to [13]). Fig. 2 presents a comparison of the characteristic velocity v_r obtained for the drying cell and the values for

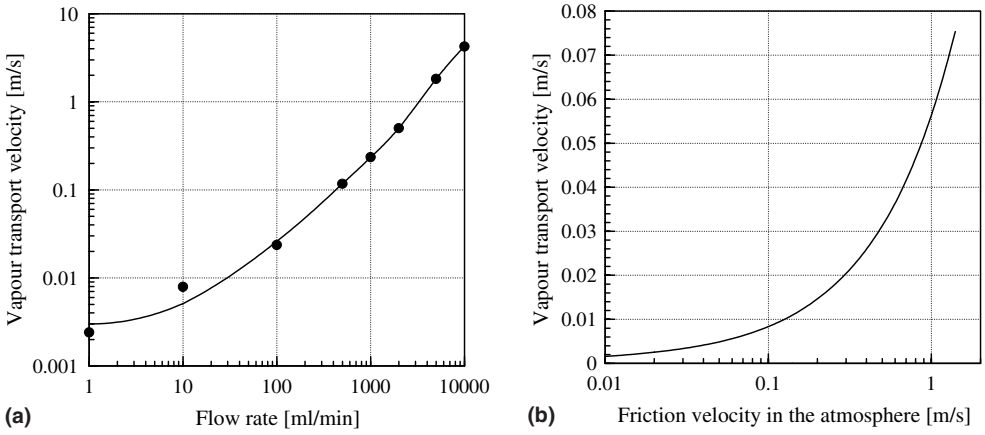

Fig. 2. Variation of the vapour transport velocity (v_r) with (a) the flow rate inside the cell (where the dots indicate the results obtained by the CFD simulations), and (b) variation of v_r with friction velocity in the atmosphere [6].

the atmosphere (based on expressions presented in [7]). By using these charts it is possible to correlate the flow rate of the air supply with a given atmospheric condition. The results obtained by this procedure will be further discussed in Section 3.1.

2.2. Experimental procedure

In this study two-dimensional and one-dimensional imaging techniques were used. While the two-dimensional images give qualitative information about the droplet shape after impingement and its variation throughout the evaporation episode, the one-dimensional images also yield quantitative information about the concentration profiles along the depth direction in the porous substrate. The concentration profiles are then used to determine the mass fraction of liquid remaining in the substrate, and the corresponding values of evaporation rate and mass flux to the air stream. Further information regarding the MRI imaging acquisition can be found in Ref. [9].

Signal losses due to T2 relaxation have been addressed in an earlier publication [9] and it was shown that the T2 of the water/glass bead system decreased by about 76% from the beginning to the end of drying (126 ms versus 30 ms). Here the DEM/glass beads system T2 value was measured to be 100 ms at the start of drying, resulting in a signal loss of around 2.5%. The T2 value at the end of drying was estimated to be around 23 ms resulting in a signal loss of around 12% at the end of drying.

Each MRI acquisition cycle comprises a one-dimensional liquid droplet profile acquisition and a two-dimensional slice selective liquid droplet image acquisition. During the full evaporation episode many such acquisition cycles are performed, generating a time series of images that is used to reconstruct the time evolution of the drying phenomenon.

Fig. 1 shows schematic representations of the two-dimensional image and the corresponding concentration profiles. As neither the Perspex cell nor the porous substrate (glass beads or sand) have a detectable NMR signal for the acquisition parameters used here, the two-dimensional images obtained display only the shape and position of the liquid droplet. One-dimensional imaging techniques give the profile of liquid concentration with depth in the substrate (along the x axis in Fig. 1), where the signal at each position is proportional to the integrated concentration along a horizontal plane of the impinged droplet. Since the amount of liquid delivered to the porous substrate is known, it is possible to correlate (normalise) the total intensity of the signal obtained by one-dimensional profiling, i.e. the integral of the signal along the entire thickness of the porous medium, with the known mass of the liquid droplet. Thus, it is possible to translate the signal intensity into liquid concentration units, and express the profile graphs (Fig. 1) as integrated concentration[1] (kg/m) versus x (m). In addition, the rate of change of the signal integrated over the entire thickness of the porous medium can provide the evaporation rate of the liquid droplet, since the total signal is proportional to the mass of liquid present in the substrate.

For imaging the field-of-view was 5 mm × 10 mm ($x \times z$) and the image size was 64 × 128 pixels, yielding an isotropic pixel resolution of 78 μm. For profiling, the field-of-view was 20 mm using 256 points along the x axis, also yielding a resolution of 78 μm. A complete description of these procedures and the imaging parameters used can be found in [11].

2.3. Parameterisation

By normalising the data obtained using characteristic values for the evaporation of a free liquid surface exposed to a similar air stream, it is possible to analyse the limiting influence of the transport inside the porous medium upon

[1] Integrated concentration is defined as liquid concentration in the porous medium integrated over the area of the horizontal plane.

the evaporation process. Accordingly, a characteristic mass flux can be estimated as (for a negligible background vapour concentration in the air stream):

$$F_0 = v_{r0} c_{sat} \tag{2}$$

where v_{r0} denotes the characteristic vapour transport velocity for a given flow rate and c_{sat} represents the value of the saturated vapour concentration in air. In order to determine the characteristic time scale, it is necessary to determine a characteristic area through which the flux F_0 transports the mass of the liquid droplet (M_0). A satisfactory magnitude for this area can be calculated by using the droplet radius prior to the impingement (r_0), since the radius of the wet spot after the impingement will be larger than r_0, but of the same order of magnitude. Therefore, the time scale of the process is defined as:

$$T_0 = \frac{M_0}{F_0 A_0} \tag{3}$$

where A_0 denotes the characteristic area ($A_0 = \pi r_0^2$).

This time scale represents the approximate time that an equivalent mass of liquid would take to evaporate from a fully saturated wet spot (i.e. a free liquid surface) with a radius equal to r_0, when exposed to the given air flow. Normalising the relevant variables of the problem by using characteristic time scale (T_0), mass (M_0) and mass flux (F_0), the following dimensionless parameters were introduced:

$$T^* = \frac{T}{T_0} \quad M^* = \frac{M}{M_0} \quad F^* = \frac{F}{F_0} \quad (\mathrm{d}M/\mathrm{d}T)^* = \frac{\mathrm{d}M/\mathrm{d}T}{F_0 A_0}$$
$$c^* = \frac{c}{c_0} \tag{4}$$

where the value of $\mathrm{d}M/\mathrm{d}T$ is the evaporation rate (kg/s) and F is the mass flux per unit area (kg/m^2 s), which is calculated as $\mathrm{d}M/\mathrm{d}T$ divided by the area of the wet spot in the surface of the porous medium exposed to the air stream. T^* denotes the non-dimensional time, M^* is non-dimensional mass, also called mass fraction remaining, and F^* and $(\mathrm{d}M/\mathrm{d}T)^*$ are the dimensionless mass flux and evaporation rate. c^* denotes non-dimensional form of the integrated concentration presented by the concentration profiles, where c is the concentration expressed in kg/m and c_0 is the characteristic concentration ($c_0 = c_{sat-liq}\ A_0$), where $c_{sat-liq}$ is the saturated liquid concentration for the porous medium.

3. Results and discussion

The investigation of the influence of the efficiency of the removal of vapour from the atmosphere/porous medium interface was carried out by varying the flow rate of the air supply for the experimental cell based on the relationships presented in Fig. 2, in an attempt to simulate different drying regimes in the atmosphere.

Ideally, the best way to analyse this influence and to compare with previous published data would be to study the evaporation of water droplets under various drying conditions, since water droplets evaporating from several porous substrates were already investigated in [9]. However, the duration of the water droplet evaporation episode is ≈2–3 h with a flow rate equal to 10 ml/min (equivalent to $u_* = 0.1$ m/s), and if the flow rate is increased to simulate u_* values in the range 0.2–1 m/s, the evaporation will proceed even quicker. This may cause considerable problems for the utilisation of NMR imaging for such investigations, since the NMR imaging techniques used in this study require at least 5 min for each droplet image to be acquired.

Therefore, in order to avoid these problems the influence of the removal of vapour from the porous medium surface is analysed using a DEM droplet. As a base configuration a DEM droplet (1.15 mm radius) was delivered to a porous substrate composed of 120 μm diameter glass beads, with an impact velocity of 0.5 m/s. The impinged spot was then exposed to a 10 ml/min air stream (v_r equal to 0.008 m/s, which is approximately equivalent to a friction velocity in the atmosphere of 0.1 m/s), which takes ≈33 h to evaporate (experiment no. 1). Subsequently, the flow rate values were varied from the base case value up to 100 and 490 ml/min (experiments no. 2 and no. 3), which represent equivalent values of $u_* = 0.25$ and 1.1 m/s, respectively.

The results presented here are divided into three main sections. In the first section, the accuracy of the simulation of the transport mechanisms through the atmosphere/porous substrate interface is analysed, and evaporation rates obtained in this work are compared to values obtained in field experiments presented in [10]. In the second section, a comparison of the drying regimes obtained for water droplets [9] and DEM droplets under similar evaporation conditions is presented. Finally, the third section, presents an analyses of the influence of the removal of vapour from the atmosphere/porous medium interface.

3.1. Mass transport in the atmosphere/porous substrate interface

In order to verify the accuracy of the simulation of the transport mechanisms through the atmosphere/porous substrate interface, the evaporation rates obtained in this work are compared to values obtained in field experiments performed by [10]. The objective of this comparison is to evaluate the inaccuracies and limitations of the present experiments in simulating evaporation in the atmosphere.

As stated earlier, the initial evaporation rate depends only on the area of the wet spot in the porous surface, the vapour pressure of the liquid and the atmospheric conditions responsible for the vapour removal from the contaminated surface, expressed in the form of the vapour transport velocity. Therefore, it is possible to correlate the evaporation rates measured in field experiments in the real atmosphere and in the NMR experiments, if the area of the wet spot on the porous surface and the vapour pressure of the liquid are known.

Roberts [10] presented detailed information about a series of field trials performed to measure the evaporation rates of liquid droplets from sand and concrete surfaces. This data set includes meteorological conditions (wind speed, friction velocity, stability conditions and air temperature), ground temperature, spread ratio measurements (spread ratio is defined as the ration between the droplet diameter prior to impingement and the diameter just after impingement) and mass fraction of liquid remaining inside the porous surface. From the 41 experiments reported, five experiments were selected, which describe the evaporation of DEM droplets from sand surfaces subjected to a friction velocity of approximately 0.10 m/s (3 trials) and 0.25 m/s (2 trials). Referring to Fig. 2, friction velocities of 0.10 and 0.25 m/s provide vapour transport velocities equivalent to those obtained in the interior of the drying cell for flow rates of 10 and 100 ml/min, respectively.

The time interval between each concentration profile acquisition in the present work varies from ≈5 to 12 min, and the evaporation rates calculated using the concentration profiles represent average values for the relevant periods. However, [10] presents evaporation data for every 1 min period. Therefore, in order to compare the 2 data sets, the results of [10] were averaged over a 5 min period for the cases with u_* equal to 0.10 m/s, and over a 12 min period for the cases with u_* equal to 0.25 m/s.

Table 1 summarises the vapour transport velocity obtained in the NMR experiment for flow rates of 10 and 100 ml/min, and the vapour transport velocity obtained in the field trials. The average ratio between the v_r values obtained in both experiments is close to 1, with and error between 10% and 15%. These values demonstrate the applicability of the technique described in this work to simulate the mass transfer inside the interfacial layer of the atmosphere, given the size limitations imposed on the experimental apparatus. The 10–15% variation is very small compared to the relatively large range of values in the field data.

3.2. Evaporation of DEM droplets

This section presents a comparison of the drying regimes obtained for water droplets [9] and DEM droplets under similar evaporation conditions. Fig. 3 presents the time evolution of the axial (x) concentration profiles of liquid for experiment no. 1, and the corresponding images of the shape of the droplet inside the porous substrate. It is important to inspect the two-dimensional images together with the one-dimensional concentration profiles, since the images provide information about the shape of the droplet, but only give limited quantitative information about the concentration of liquid inside the substrate. The profiles provide the complementary information concerning the concentration levels.

The first image presented in Fig. 3 represents the shape of the droplet just after impingement. However, it should be noted that the acquisition of the image presented in Fig. 3 started 1 min after the droplet delivery, since before the image acquisition there is a one-dimensional concentration profile acquisition. In addition, the total imaging time in this case is ≈12 min. Therefore, this image represents an integrated view of the impinged droplet over this period of time, and any variation in its shape during this period is not resolved. This time interval is negligible in comparison with the total duration of the evaporation episode $T^* \approx 0.8$ (≈2100 min)—as will be discussed later.

It can be seen that the shape inside the porous medium is similar to a half-spheroid, similar to the results presented in [9] for water droplets. The fairly definite shape indicates that the droplet exists as a fully saturated region with a relatively sharp interface. It is possible to clearly distinguish the position of the surface of the substrate, indicated by the flat region on the upper side of the droplet. It should be noted that the upper surface of the droplet is not completely flat. These irregularities are caused by disturbances of the glass beads due to the impact with the liquid droplet, forming a small crater on the surface of the substrate. In fact, the crater formed by the disruption of the glass beads is even more noticeable for the DEM droplet impinged in 120 μm glass beads than it is for the water droplet, as presented in reference [9]. This may be related to that fact that the viscosity of DEM is larger than that of water, which may cause larger shear stress on the surface of the glass beads, increasing the forces disturbing the particles.

As the droplet evaporation begins, drying starts from the upper surface of the droplet, as can be clearly observed by the reduction in the concentration levels of the profiles in the region closer to the surface. While there is a considerable reduction in the concentration level close to the surface, the concentration in the deeper layers of the substrate remains practically unaltered. This is shown by the change in the shape of the concentration profiles and by the significant reduction in the concentration close to the surface observable in the images.

This behaviour was not observed for the evaporation of water droplets, as reported by [9]. In fact, it was reported

Table 1
Comparison of the vapour transport velocity values obtained in the NMR experiment and in the field trials

Flow rate (ml/min)	Equivalent friction velocity (m/s)	Vapour transport velocity inside the drying cell (±range) (mm/s)	Vapour transport velocity at the atmosphere (±s.d.) (mm/s)	Average ratio (v_r(cell)/v_r(atm.))
10	0.10	7.0 ± 0.4	6.0 ± 1.7	1.11
100	0.25	11.4[a]	13.0 ± 3.1	0.86

[a] The error bars denote the range of the data. There is only one experiment available from the present experimental work for the v_r value equivalent to $u_* = 0.25$ m/s, and so no range value is available.

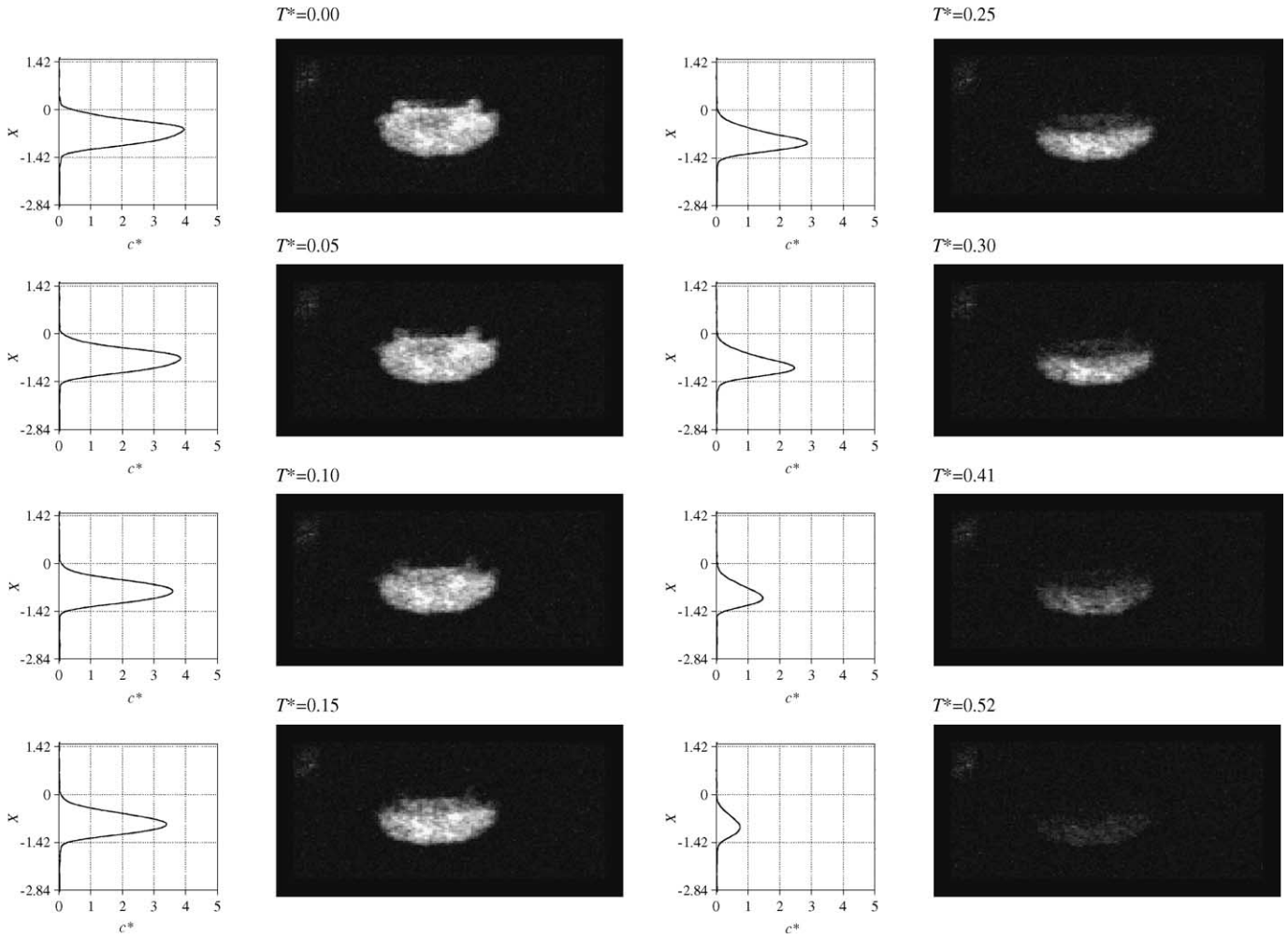

Fig. 3. Time evolution of the concentration profiles of liquid and images of the shape of the droplet inside the porous substrate (flow rate = 10 ml/min).

that after the initial stages of the evaporation of water droplets, during which the concentration is reduced mainly in the region close to the surface, the liquid concentration was reduced approximately evenly across the full depth of the liquid region, which suggested that the liquid is migrating from the deeper layers of the substrate to the upper layers, probably due to capillary diffusion. In these circumstances the receding evaporation-front behaviour (assumed in some droplet evaporation models [1,7] and [10]) is not applicable. By contrast, the results obtained here for DEM droplet clearly indicate a progression of a receding concentration front inside the substrate, which is evident in the images.

This behaviour can be related to the fluid motion due to capillary action during the evaporation episode. The main differences between the relevant properties of DEM and water are related to the viscosity (4.00×10^{-3} kg/m s for DEM and 1.27×10^{-3} kg/m s for water) and surface tension coefficient (3.24×10^{-2} N/m for DEM and 6.80×10^{-2} N/m for water). According to [12] the mass diffusivity of liquids in porous media is inversely proportional to the liquid viscosity, and directly proportional to the capillary pressure value, which is proportional to the surface tension value of the liquid. Thus, the increased viscosity and reduced surface tension of DEM in relation to water contribute to smaller values of the mass diffusivity of the DEM inside the porous medium. Although this analysis may be over simplistic, since the mass diffusivity may be dependent on other parameters (such as contact angle, for instance), it is consistent with the behaviour presented by the images and concentration profiles.

However, this receding front does not progress through the entire droplet depth. The front recedes to approximately half of the droplet depth (Fig. 3, images and profiles obtained until $T^* = 0.25$), and from this point the droplet starts to evaporate homogeneously (Fig. 3, images and profiles obtained after $T^* = 0.25$). This may indicate that the liquid redistribution due to capillary action is not strong enough to supply liquid to the surface at a rate large enough to maintain the high concentration levels close to the surface, where the evaporation is larger. However, as the drying proceeds the evaporation rate becomes small enough that the evaporative flux is balanced by liquid motion, and the droplet starts to dry homogeneously.

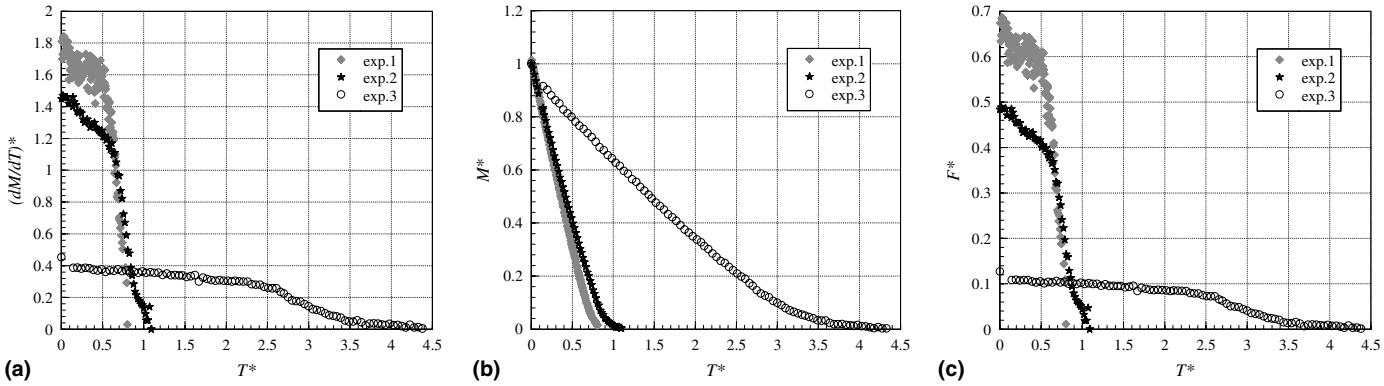

Fig. 4. (a) Non-dimensional evaporation rate $(dM/dT)^*$ of the droplet versus T^*, (b) mass fraction of liquid remaining inside the substrate based on the integration of the concentration profiles and (c) non-dimensional mass flux (F^*) versus T^*.

This can also be observed in Fig. 4(a), which presents the complete evaporation rate event of the droplet. In spite of the levels of noise found in the curves of evaporation rate and mass flux, it is possible to observe a gentle reduction of the evaporation rate from the initial stages until T^* approximately equal to 0.2. From this point the evaporation rate presents a nearly constant value, which coincides with the period when the droplets evaporate homogeneously. This may indicate that the liquid redistribution, due to capillary action, is strong enough to balance the evaporative flux, and thus maintaining the value of the evaporation rate.

In fact, evaporation occurs along the entire boundary of the droplet, even in the deeper layers of the porous medium. As the conversion from one phase to the other proceeds, the concentration of vapour inside the substrate is increased. If these vapours are not removed, the vapour concentration inside the pores will increase until it reaches saturation levels. Closer to the surface, there is less resistance to vapour migration (or diffusion) to the air stream above. However, in the deeper layers, vapour diffusion is limited by a large layer of the substrate. As a consequence, there is an increase in the vapour concentration in the substrate, which limits the phase change. This behaviour produces a larger evaporation rate in the upper region of the impinged droplet, and less in the deeper layers of the substrate, which physically explains the impression of "drying from the top" as shown by the impinged droplet images. This behaviour is further explored in Section 3.3.

3.3. Influence of the removal of vapour from the atmosphere/porous medium interface

This section presents the analyses of the influence of the efficiency of the removal of vapour from the atmosphere/porous medium interface. As stated previously, 3 different experiment configurations were tested, in which the impinged spot was exposed to a 10 ml/min air stream (experiment no. 1), a 100 ml/min air stream (experiment no. 2) and a 490 ml/min air stream (experiment no. 3), corresponding to equivalent values of $u_* = 0.10$, 0.25 and 1.1 m/s, respectively.

Figs. 5 and 6 present the time evolution of the concentration profiles of liquid and images of the shape of the DEM droplet inside the porous substrate for each additional configuration tested, i.e. experiment nos. 2 and 3 (100 and 490 ml/min, respectively). The three experiments (1, 2 and 3) show similar behaviour with the concentration at the surface dropping very rapidly, but after a certain period of time the concentration levels become nearly constant, and the droplet evaporates quasi-homogeneously. The main difference in the results obtained for the three configurations is the drying rate. For instance, images and profiles for experiment no. 1 show very small concentration levels remaining at $T^* = 0.5$, while the values for experiment no. 2 are considerably larger. The values for experiment no. 3 at $T^* = 0.5$ are very similar to those obtained at $T^* = 0.0$, which indicates that very little signal was lost. In fact, clear images are still obtained at $T^* = 2.0$, for experiment no. 3. However, one must be aware that the time scale for each configuration is very different, since there is a large difference in the mass flux to the air stream. The times scales are ≈3082, 1028 and 208 min, for experiments nos. 1, 2 and 3, respectively.

The duration of the evaporation episode (in minutes) is much smaller for the configurations using a larger flow rate. However, the non-dimensional evaporation time (T^*) represents a time scale relative to the evaporation of a saturated pool of liquid with a radius equal to r_0. Accordingly, although the droplets in experiments nos. 2 and 3 evaporate physically faster, the results obtained indicate that they evaporate significantly slower than the evaporation of a saturated pool of liquid, which indicates the strong limiting effect of the porous medium transport upon the evaporation process. The transport mechanisms in the interior of the porous medium restrict the liquid supply to the surface and the vapour motion through the porous matrix, limiting the mass flux to the air stream and the evaporation rate of the liquid droplet.

This behaviour can be more clearly visualised in Fig. 4(b), which presents the time evolution of the mass

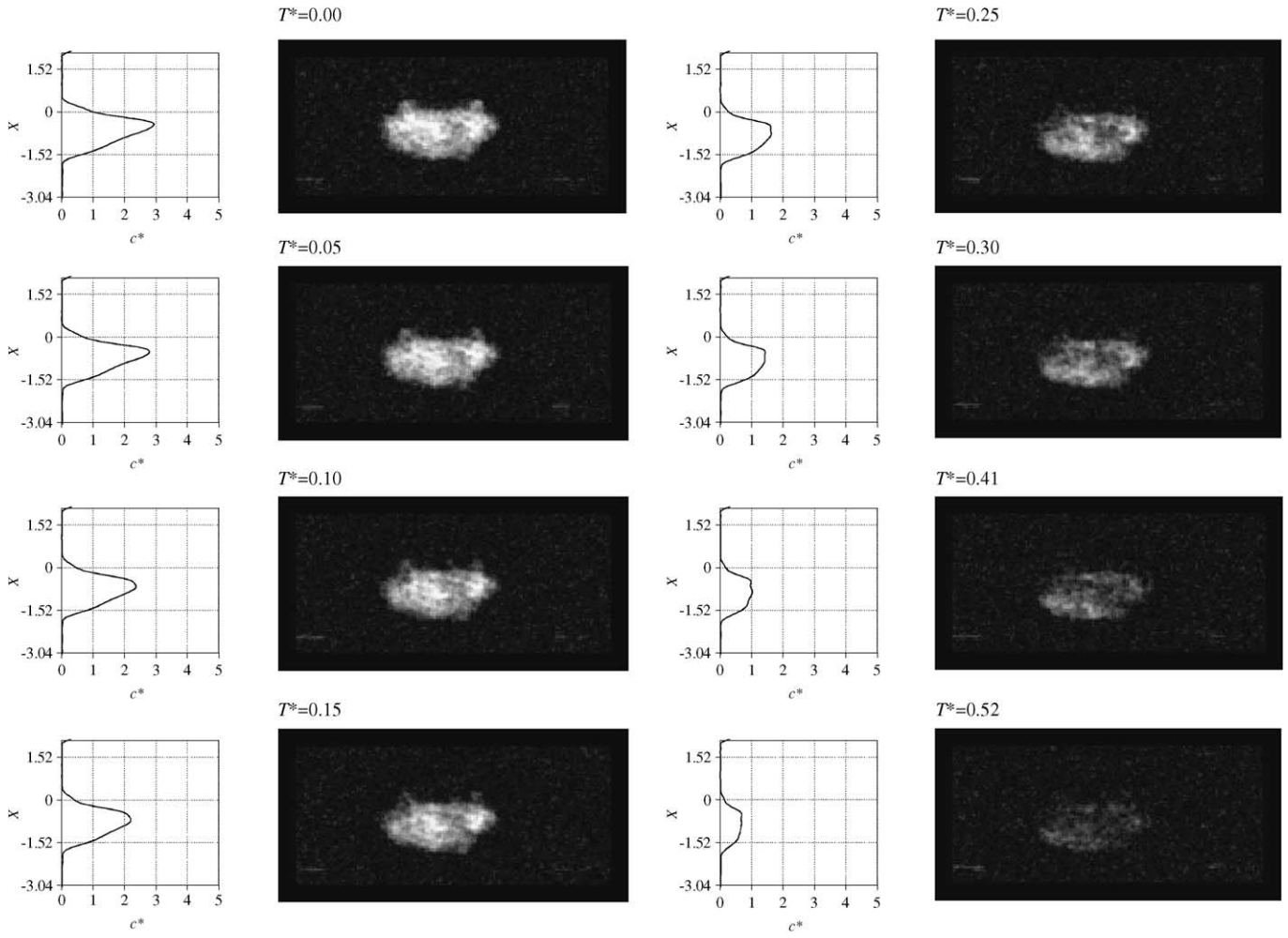

Fig. 5. Time evolution of the concentration profiles of liquid and images of the shape of the droplet inside the porous substrate (flow rate = 100 ml/min).

fraction of liquid remaining in the substrate. It is evident that the evaporation episode for a flow rate of 10 ml/min lasts until approximately $T^* = 0.8$, while that for a flow rate of 100 ml/min lasts until approximately $T^* = 1.1$, and that for a flow rate of 490 ml/min lasts until approximately $T^* = 4.0$.

These evaporation times are directly related to the values of the evaporation rate displayed in Fig. 4(a). Fig. 4(a) and (b) show a drying behaviour very similar for the three configurations, in that there is a distinct period of slowly decreasing evaporation rate, followed by a more rapid decrease in the evaporation rate, due to the reduction of the mass fraction of liquid remaining in the substrate.

In spite of the similarities in the shapes of the curves, the values of evaporation rate are quite different for each situation. In absolute terms, the mass flux to the air stream is larger for the configurations with larger flow rates; however, they represent only a small fraction of the values for a saturated wet spot. The value of F^* represents the mass flux to air stream per unit area normalized by the mass flux of a fully saturated wet spot exposed to a similar air flow. Even in the first few instants of the evaporation episode the value of F^* is significantly lower than 1 for all experiments. As the flow rate of the air stream above the surface increases, the values of F^* are reduced. Although liquid droplets tend to evaporate faster when exposed to a more efficient removal of vapour from the surface, the porous media transport is not significantly altered from one configuration to the other (since liquid and porous medium properties are the same for all three configurations), as a consequence, the limiting effects of the porous medium are even more evident when exposed to a more efficient removal of vapour from the surface.

4. Concluding remarks

Analyses of data from magnetic resonance imaging (MRI) studies of the evaporation of liquid droplets from porous surfaces are presented. DEM droplets are initially embedded in the porous substrate by impingement, and are then evaporated over a period of several hours, the surface of the substrate being ventilated by a controlled airflow. The data obtained include images of impinged

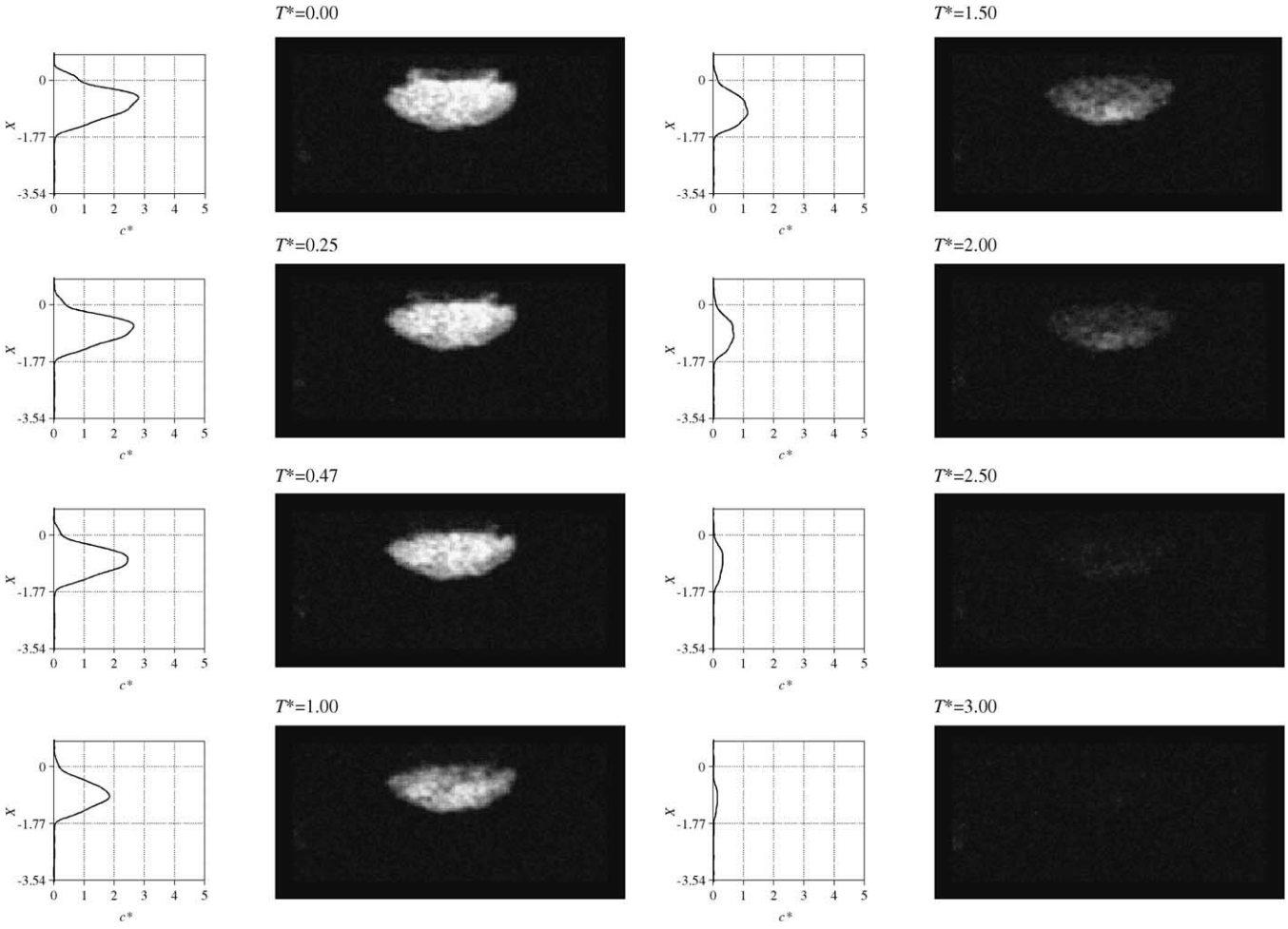

Fig. 6. Time evolution of the concentration profiles of liquid and images of the shape of the droplet inside the porous substrate (flow rate = 490 ml/min).

droplets inside the porous substrate and their variation during evaporation, as well as one-dimensional concentration profiles through the substrates, and time evolution of the mass fraction of liquid remaining and corresponding evaporation rates.

Comparisons with previously published work, using water droplets, were performed in order to evaluate the influence of the liquid properties on the drying process. The results suggest that liquid properties, such as viscosity and surface tension, significantly affect the liquid diffusion in the porous medium, altering the drying regime.

In order to evaluate the influence of the airflow in the surface of the porous medium, different experimental configurations are tested by varying the speed of the flow stream above the porous surface. The results obtained show that although liquid droplets tend to evaporate faster and present larger evaporation rates when exposed to a more efficient removal of vapour from the surface, the limiting effects of the porous medium are even more evident.

It is apparent from this study that there is still a considerable amount of both experimental and theoretical work still required. In particular, it would be desirable to extend the scope of the experimental studies to encompass a wider range of liquid and substrate properties, i.e. liquid viscosity, temperature, wetting properties of liquid solid interface, and to use the results to establish the parameters that characterise the different regimes of transport behaviour in the substrate. This should enable some better definition of the range of conditions in which the receding evaporation-front assumption can be used.

Acknowledgements

The authors wish to acknowledge the sponsorship of the Brazilian Government through CAPES (Fundação Coordenação de Aperfeiçoamento de Pessoal de Nível Superior) and DERA (Defence Evaluation and Research Agency—Porton Down, United Kingdom) under Agreement Number CU013-0000002229.

References

[1] R.F. Griffiths, I.D. Roberts, Droplet evaporation from porous surfaces, model validation from field and wind tunnel experiments for sand and concrete, Atmos. Environ. 33 (1999) 3531–3549.

[2] K. Wallace, K. Yoshida, Determination of dynamic spread factor of water droplets impacting on water-sensitive paper surfaces, J. Coll. Int. Sci. 63 (1978) 164–165.
[3] J.F. Oliver, Initial stages of inkjet drop impaction, spreading, and wetting on paper, TAPPI J. 67 (1984) 90–94.
[4] J.F. Oliver, L. Agbezuge, K. Woodcock, A diffusion approach for modelling penetration of aqueous liquids into paper, Colloids Surf. A: Physicochem. Eng. Aspects 89 (1994) 213–226.
[5] W. Cooper, F.H. Hardaway, L. Edwards, The evaporation of two thickened agent simulants from wet and dry concrete, Report No. CRDEC-TR-86033, CRDEC, Aberdeen Proving Ground, Aberdeen, MD, USA (1986).
[6] W. Cooper, F.H. Hardaway, L. Edwards, The evaporation of two thickened agent simulants from wet and dry sand, Report No. CRDEC-TR-112, CRDEC, Aberdeen Proving Ground, Aberdeen, MD, USA (1990).
[7] I.D. Roberts, R.F. Griffiths, A Model for the evaporation of droplets from sand, Atmos. Environ. 29 (1995) 1307–1317.
[8] S.N. Westin, S. Winter, E. Karlsson, A. Hin, F. Oeseburg, On modelling of the evaporation of warfare agents on the ground, J. Hazardous Mat. A 63 (1998) 5–24.
[9] N.C. Reis, R.F. Griffiths, M.D. Mantle, L.F. Gladden, Investigation of the evaporation of embedded liquid droplets from porous surfaces using magnetic resonance imaging, Int. J. Heat Mass Transfer 46 (7) (2003) 1279–1292.
[10] I.D. Roberts, The evaporation of neat/thickened agent simulant droplets from porous surfaces, Final report on agreement No. 2044/013/CDBE, UMIST, 1996.
[11] M.D. Mantle, N.C. Reis, R.F. Griffiths, L.F. Gladden, MRI studies of the evaporation of a single liquid droplet from porous surfaces, Magn. Reson. Imaging 21 (3–4) (2003) 293–297.
[12] B. Wang, W. Yu, A method for evaluation of heat and mass transport properties of moist porous media, Int. J. Heat Mass Transfer 31 (1988) 1005–1009.
[13] N.C. Reis, Droplet impingement and evaporation from porous surfaces, PhD Thesis, UMIST, 2000.